IEEE Access
Multidisciplinary | Rapid Review | Open Access Journal

Received 7 October 2023, accepted 14 October 2023, date of publication 19 October 2023, date of current version 26 October 2023.

Digital Object Identifier 10.1109/ACCESS.2023.3325911

RESEARCH ARTICLE

Non-Integer Order Generalized Filters Designs

JULIA NAKO[1], (Graduate Student Member, IEEE), COSTAS PSYCHALINOS[1], (Senior Member, IEEE), AHMED S. ELWAKIL[2,3,4], (Senior Member, IEEE), AND SHAHRAM MINAEI[5], (Senior Member, IEEE)

[1]Electronics Laboratory, Department of Physics, University of Patras, Rio, 26504 Patras, Greece
[2]Department of Electrical and Computer Engineering, University of Sharjah, Sharjah, United Arab Emirates
[3]Department of Electrical and Software Engineering, University of Calgary, Alberta, AB T2N 1N4, Canada
[4]Nanoelectronics Integrated Systems Center (NISC), Nile University, Giza 12588, Egypt
[5]Department of Electrical and Electronics Engineering, Dogus University, Umraniye, 34775 Istanbul, Turkey

Corresponding author: Costas Psychalinos (cpsychal@upatras.gr)

This work was supported by HEAL-Link.

ABSTRACT Non-integer order filters can be derived from a generalized structure presented in this work. More specifically, fractional-order and power-law filters of single- or double-order are special cases of non-integer order filters with three degrees of freedom and can be implemented using a Current Feedback Operational Amplifier as the active element. The transfer function is formed as a ratio of two impedances which can be synthesized using Foster or Cauer RC networks. A curve-fitting based technique is employed for approximating the magnitude and phase of each impedance. The behavior of the presented structures is evaluated through simulation results, using the OrCAD design suite and, also, through experimental results.

INDEX TERMS Analog filters, current feedback operational amplifiers, generalized filters, fractional-order filters, non-integer order filters, power-law filters.

I. INTRODUCTION

Non-integer order filters offer improved design flexibility due to the extra degrees of freedom resulting from the multiple non-integer orders. The design flexibility appears in the scaling of the realized time constants, as well as in the fine adjustment of the roll-off value in the transition between the characteristic bands of the filters [1], [2]. There are two main sub-categories of these filters: a) fractional-order filters with transfer functions formed by using non-integer Laplacian operators [3], [4], [5], [6], [7], [8], [9], [10], [11], and b) power-law filters with transfer functions derived by raising the conventional integer order transfer functions to a (non-integer) exponent [12], [13], [14]. Although filters of the first sub-category can be theoretically implemented using fractional-order capacitors, in practice this is not possible, as their market availability does not yet easily exist [15]. Therefore, both filter categories are usually implemented using suitable approximation techniques where rational integer-order transfer functions are derived and realized through classical filter synthesis techniques. In order to implement fractional-order filters, well-known approximation tools, such as the Oustaloup method and the continued fraction expansion tools, could be employed. These methods, however, cannot be used for realizing power-law filters. A solution for overcoming this obstacle is to use a curve-fitting based method, where both the magnitude and phase responses of the transfer function are used in order to derive an equivalent integer-order approximation function [12], [16]. It must be mentioned at this point that this method is also applicable in the case of fractional-order filter functions.

The implementation of the resulting approximate transfer functions can be performed using, for example, multi-feedback structures based on active elements with electronically controllable characteristics (e.g., Operational Transconductance Amplifiers-OTAs) resulting in structures with electronic tunability of the filter frequency characteristics. However, this solution suffers from the increased circuit complexity and, consequently, from high power dissipation [1]. An attractive alternative solution has been introduced in [17], where the approximation transfer function

The associate editor coordinating the review of this manuscript and approving it for publication was Fabian Khateb.

is expressed as a ratio of two impedances which are generally frequency dependent. This concept was applied for approximating fractional-order Butterworth and Chebyshev filter functions, as well as for implementing fractional-order controllers [18].

The contribution made in this work is the further generalization of this concept in order to derive in a systematic manner the elementary fractional-order and power-law filter functions, with minimum active component count. More specifically, a generalized transfer function with three degrees of freedom is introduced and its implementation is performed using only one Current Feedback Operational Amplifier (CFOA) as the active element. Minimization of the active component count is achieved by expressing the approximation transfer function as a ratio of two impedances and their choice is performed taking into account the frequency behavior of the Foster/Cauer RC networks [19]. One of the offered features is that the kind of the filter function (i.e., fractional-order or power-law) is determined by one of the employed impedances, while the type of the filter function (i.e., low-pass, high-pass, band-pass) is determined by the second impedance. Another important feature is that the corresponding inverse filter functions are easily implementable simply by interchanging the impedances in the main core. This evidently provides design flexibility and versatility in the introduced structure. Finally, the presented generalized filter structure has a high-impedance input and a low-impedance output and, consequently, it is cascadable without requiring extra buffer stages. The only practical drawback is the absence of on-the-fly adjustability of their characteristics, in the sense that the whole network must be re-designed for any different filter function. This is the price paid for the achieved non-integer order filter and minimization of the active and passive component count. The structures which offer electronic tunability suffer from the increased number of active components.

The paper is organized as follows: a brief description of the elementary fractional-order and power-law filter functions is given in Section II, while the generalized transfer functions of non-integer order filters are given in Section III in tabular form. The single active element implementation of the generalized filter is presented in Section IV and the performances of the resulting special cases of filters are evaluated in Section V through simulation results using OrCAD and the model of the Analog Devices AD844 CFOA device, as well as through experimental results.

II. NON-INTEGER ORDER FILTERS

A. FRACTIONAL-ORDER FILTERS

The transfer function of a fractional-order low-pass filter, of order $0 < \alpha < 1$, is described by the transfer function given in (1)

$$H_{LP,FO}(s) = G_0 \frac{1}{(\tau s)^{\alpha} + 1}, \tag{1}$$

where the time constant τ determines the pole frequency (ω_p) according to the formula $\tau = 1/\omega_p$, and G_0 is the gain of the filter.

Substituting the Laplacian operator by the formula: $s^{\alpha} = \omega^{\alpha}[\cos(0.5\pi\alpha) + j\sin(0.5\pi\alpha)]$, the gain response of the filter is the given by

$$| H_{LP,FO}(\omega) | = G_0 \frac{1}{\left[1 + (\omega\tau)^{2\alpha} + 2(\omega\tau)^{\alpha}\cos(0.5\pi\alpha)\right]^{1/2}}. \tag{2}$$

Defining as *knee* frequency (ω_k) the frequency where a specific drop from the maximum gain of the filter occurs, then using (2), the -3dB *knee* frequency of the filter is associated with the pole frequency according to (3)

$$\omega_{k,LP,FO} = \omega_p \left[\sqrt{1 + \cos^2(0.5\pi\alpha)} - \cos(0.5\pi\alpha)\right]^{1/\alpha}. \tag{3}$$

Therefore, scaling of the *knee* frequency can be performed by using the order of the filter α whereas in the case of integer-order filters, the pole frequency is always equal to the *knee* frequency. The slope of the transition between the pass-band and the stop-band of the filter is -20α dB/dec., and the range of the phase response is $[0, -\alpha\pi/2]$.

Considering a fractional-order high-pass filter with maximum gain G_0, its transfer function and gain response are given by (4)–(5), respectively

$$H_{HP,FO}(s) = G_0 \frac{(\tau s)^{\alpha}}{(\tau s)^{\alpha} + 1}, \tag{4}$$

$$| H_{HP,FO}(\omega) | = G_0 \frac{(\omega\tau)^{\alpha}}{\left[1 + (\omega\tau)^{2\alpha} + 2(\omega\tau)^{\alpha}\cos(0.5\pi\alpha)\right]^{1/2}}. \tag{5}$$

The expression of the *knee* frequency is given by

$$\omega_{k,HP,FO} = \omega_p \left[\sqrt{1 + \cos^2(0.5\pi\alpha)} + \cos(0.5\pi\alpha)\right]^{1/\alpha}. \tag{6}$$

The *knee* frequency is located at a relatively higher frequency than that of the pole frequency, which is the opposite case when compared to the *knee* frequency of the low-pass filter. The transition from the stop-band to the pass-band of the filter is described by a slope of $+20\alpha$ dB/dec., while the phase is within the range $[\alpha\pi/2, 0]$.

An important type of fractional-order function can be derived by considering that the order of the numerator in (4) is not equal to the order of its denominator. The resulting transfer function is given by (7)

$$H_{BP,FO}(s) = G_0 \frac{(\tau s)^{\beta}}{(\tau s)^{\alpha} + 1}, \tag{7}$$

with $0 < \beta < \alpha < 1$, τ being the time constant, and G_0 is a scaling factor for adjusting the gain of the filter at the peak frequency in a desired level.

The gain response of this filter is given by (8)

$$| H_{BP,FO}(\omega) |= \frac{(\omega\tau)^{\beta}}{\left[1+(\omega\tau)^{2\alpha}+2(\omega\tau)^{\alpha}\cos(0.5\pi\alpha)\right]^{1/2}}. \tag{8}$$

This is actually an asymmetric band-pass filter with a slope equal to $+20\beta$ dB/dec., in the low-frequency range, and equal to -20(α- β) dB/dec., in the high frequency range. The phase angle lies within the range $[+\beta\pi/2, -(\alpha-\beta)\pi/2]$. Defining as peak frequency (ω_{peak}) the frequency where a maximum/minimum of the frequency response occurs and by solving the equation $d/d\omega \mid H_{BP,FO}(\omega) \mid_{\omega=\omega_{peak}} = 0$, the associated lower and upper *knee* frequencies ($\omega_{k,l}$, $\omega_{k,h}$) can be obtained by solving the following non-linear equation: $\mid H_{BP,FO}(\omega) \mid_{\omega=\omega_{k,l},\omega_{k,h}} = \frac{1}{\sqrt{2}} \mid H_{BP,FO}(\omega) \mid_{\omega=\omega_{peak}}$. The maximum gain ($G_{max}$) is calculated as $G_{max} = \mid H_{BP,FO}(\omega) \mid_{\omega=\omega_{peak}}$, and the bandwidth of the filter is equal to $\omega_{k,h}-\omega_{k,l}$.

Meanwhile, the transfer functions of the inverse counterparts of the aforementioned filters are [20], [21], [22], [23], [24]

$$H'_{LP,FO}(s) = G_0\left[(\tau s)^{\alpha}+1\right], \tag{9}$$

$$H'_{HP,FO}(s) = G_0\frac{(\tau s)^{\alpha}+1}{(\tau s)^{\alpha}}. \tag{10}$$

The *knee* frequencies (i.e., the frequencies where a +3dB rise from the minimum gain is observed) are given by (3) and (6), respectively. The associate gain responses are the inverse ones of those given by (2) and (5), leading also to slopes which are the inverse ones of those observed in the cases of low-pass and high-pass filters. In addition, their phase responses are the opposite of their non-inverse counterparts.
Also, the inverse band-pass filter is described by the transfer function in (11)

$$H'_{BP,FO}(s) = G_0\frac{(\tau s)^{\alpha}+1}{(\tau s)^{\beta}}, \tag{11}$$

and the peak frequency and the minimum gain of the filter are calculated under the same conditions previously mentioned, while the lower and upper *knee* frequencies ($\omega_{k,l}$, $\omega_{k,h}$) are calculated by modifying the corresponding condition as: $\mid H_{BP-FO}(\omega) \mid_{\omega=\omega_{k,l},\omega_{k,h}} = \sqrt{2} \mid H_{BP-FO}(\omega) \mid_{\omega=\omega_{peak}}$.
The slopes of the transition between the two characteristic bands of the filters are the opposite ones of those in the cases of regular filters, while the phase responses have an inverted sign, lying in the range $[0, \alpha\pi/2]$ for the inverse low-pass filter, $[-\alpha\pi/2, 0]$ for the inverse high-pass filter and $[-\beta\pi/2, +(\alpha-\beta)\pi/2]$ for the band-pass filter.

B. POWER-LAW FILTERS

A power-law low-pass filter, of order $0 < \gamma < 1$, is described by the transfer function

$$H_{LP,PL}(s) = G_0\frac{1}{(\tau s+1)^{\gamma}}, \tag{12}$$

where the variables G_0 and τ have the same meaning as in the case of fractional-order filters.
Setting $s = j\omega$ in (12), the expression of the gain becomes

$$| H_{LP,PL}(\omega) |= G_0\frac{1}{\left[1+(\omega\tau)^2\right]^{\gamma/2}}, \tag{13}$$

leading to the *knee* frequency of the filter

$$\omega_{k,LP,PL} = \omega_p\sqrt{2^{1/\gamma}-1}. \tag{14}$$

Therefore, a scaling of the *knee* frequency of the filter is also possible. The values of the slope of the transition between the two characteristics bands of the filter, as well as the range of the phase response are respectively -20γ dB/dec. and [0, $-\gamma\pi/2$].

Meanwhile, a power-law high-pass filter function has a transfer function given by (15)

$$H_{HP,PL}(s) = G_0\left(\frac{\tau s}{\tau s+1}\right)^{\gamma}, \tag{15}$$

with the expressions of the gain response and of the *knee* frequency (which is also a scaled version of the pole frequency) respectively given by

$$| H_{HP,PL}(\omega) | = G_0\frac{(\omega\tau)^{\gamma}}{\left[1+(\omega\tau)^2\right]^{\gamma/2}}. \tag{16}$$

$$\omega_{k,HP,PL} = \frac{\omega_p}{\sqrt{2^{1/\gamma}-1}}. \tag{17}$$

The values of the slope of the transition between the two characteristic bands of the filter is equal to $+20\gamma$ dB/dec., while the range of the phase response is $[+\gamma\pi/2, 0]$.

The transfer function in (18)

$$H_{BP,PL}(s) = G_0\left[\frac{(\tau s)^{\beta}}{\tau s+1}\right]^{\gamma}, \tag{18}$$

represents an asymmetric band-pass filter in the case that $0 < \beta, \gamma < 1$, and τ is the time constant. The transition slope is equal to $+20\beta\gamma$ dB/dec., in the low-frequency range, and equal to $-20(1-\beta)\gamma$ dB/dec. in the high frequency range. The phase angle is within the range $[+\beta\gamma\pi/2, -(1-\beta)\gamma\pi/2]$.

The corresponding transfer functions for the power-law inverse low-pass, high-pass and band-pass filters are respectively

$$H'_{LP,PL}(s) = G_0(\tau s+1)^{\gamma}, \tag{19}$$

$$H'_{HP,PL}(s) = G_0\left(\frac{\tau s+1}{\tau s}\right)^{\gamma}, \tag{20}$$

$$H'_{BP,PL}(s) = G_0\left[\frac{\tau s+1}{(\tau s)^{\beta}}\right]^{\gamma}, \tag{21}$$

with the *knee* frequencies of low-pass and high-pass filter given by (14) and (17). The characteristic frequencies of the inverse band-pass filter are calculated under the same conditions as in the case of fractional-order filters.

III. GENERALIZED NON-INTEGER ORDER FILTERS FUNCTIONS

Inspecting the transfer functions in (1) and (12), it is readily obtained that a generalized non-integer order low-pass filter is described by (22), with $0 < \alpha, \gamma < 1$

$$H_{LP}(s) = G_0 \left[\frac{1}{(\tau s)^{\alpha} + 1}\right]^{\gamma}, \tag{22}$$

with the expression of the gain response being

$$|H_{LP}(\omega)| = G_0 \frac{1}{\left[1 + (\omega\tau)^{2\alpha} + 2(\omega\tau)^{\alpha}\cos(0.5\pi\alpha)\right]^{\gamma/2}}. \tag{23}$$

Using (23), the *knee* frequency of the filter will be given by

$$\omega_{k,LP} = \omega_p \left[\sqrt{2^{1/\gamma} - \sin^2(0.5\pi\alpha)} - \cos(0.5\pi\alpha)\right]^{1/\alpha}. \tag{24}$$

The values of the slope of the transition between the two characteristics bands of the filter, as well as the range of the phase response are $-20\alpha\gamma$ dB/dec. and $[0, -\alpha\gamma\pi/2]$, respectively. The transfer function of the associated inverse filter is given as

$$H'_{LP}(s) = G_0[(\tau s)^{\alpha} + 1]^{\gamma}. \tag{25}$$

In a similar way, the transfer function of a generalized non-integer order high-pass filter derived from (4) and (15) becomes

$$H_{HP}(s) = G_0 \left[\frac{(\tau s)^{\alpha}}{(\tau s)^{\alpha} + 1}\right]^{\gamma}, \tag{26}$$

and the expression of the gain response is

$$|H_{HP}(\omega)| = G_0 \frac{(\omega\tau)^{\alpha\gamma}}{\left[1 + (\omega\tau)^{2\alpha} + 2(\omega\tau)^{\alpha}\cos(0.5\pi\alpha)\right]^{\gamma/2}}. \tag{27}$$

The *knee* frequency of the filter, derived from (27), is given by

$$\omega_{k,HP} = \frac{\omega_p}{\left[\sqrt{2^{1/\gamma} - \sin^2(0.5\pi\alpha)} - \cos(0.5\pi\alpha)\right]^{1/\alpha}}. \tag{28}$$

Therefore, the roll-off of the frequency response is $+20\alpha\gamma$ dB/dec. and the range of the frequency response is $[+\alpha\gamma\pi/2, 0]$.
The inverse filter function is

$$H'_{HP}(s) = G_0 \left[\frac{(\tau s)^{\alpha} + 1}{(\tau s)^{\alpha}}\right]^{\gamma}. \tag{29}$$

An important feature offered by the filters in (22), (25), (26) and (29) is that they have two degrees of freedom α and γ. As the roll-off of the frequency response is equal to $\mp 20\alpha\gamma$ dB/dec. and the *knee* frequency also depends on both orders, it is possible to independently determine these characteristics of the filter. This is not in the case of fractional-order or power-law filters, because of the existence of only one degree of freedom [25].

Generalizing (7) and (18), the resulting transfer function is given by (30)

$$H(s) = G_0 \left[\frac{(\tau s)^{\beta}}{(\tau s)^{\alpha} + 1}\right]^{\gamma}, \tag{30}$$

with $\beta \leq \alpha$, $0 \leq \alpha, \beta, \gamma \leq 1$, and τ being the time constant, with its inverse counterpart given by (31)

$$H'(s) = G_0 \left[\frac{(\tau s)^{\alpha} + 1}{(\tau s)^{\beta}}\right]^{\gamma}. \tag{31}$$

The transfer functions in (30) and, accordingly, in (31) are the most general for describing the behavior of non-integer order elementary filter functions of various kinds (i.e., fractional-order, power-law) and types (i.e., low-pass, high-pass, and band-pass). More specifically,

- The fractional-order low-pass, high-pass, and band-pass filter transfer functions in (1), (4), (7) are derived from (30) by setting $\beta = 0$ and $\gamma = 1$, $\alpha = \beta$ and $\gamma = 1$, $\gamma = 1$, $\beta < \alpha$ and $\gamma = 1$, respectively.
- The power-law filters low-pass, high-pass, and band-pass filter functions, described by (12), (15), and (18) are derived from (30) by setting $\alpha = 1$ and $\beta = 0$, $\alpha = 1$ and $\beta = 1$, $\alpha = 1$, respectively.
- The generalized non-integer order low-pass and high-pass filters in (22) and (26) are derived from (30) by setting $\beta = 0$, $\alpha = \beta$, respectively.
- The generalized non-integer order band-pass filter is that described by (30) with $\beta < \alpha$.
- The inverse counterparts of all the aforementioned filter functions are derived by the same conditions, applied alternatively in the transfer function in (31).

In order to facilitate the reader, the aforementioned findings are summarized in Table 1.

TABLE 1. Values of orders (α, β, γ) of the transfer function in (30) for implementing different types of non-integer order filter functions and their inverse counterparts starting from (30) or (31), respectively.

Filter	Variable α	Variable β	Variable γ
FO-LP in (1)	$\in (0, 1)$	0	1
FO-HP in (4)	$\in (0, 1)$	α	1
FO-BP in (7)	$\in (0, 1)$	$\in (0, 1)$ and $\beta < \alpha$	1
PL-LP in (12)	1	0	$\in (0, 1)$
PL-HP in (15)	1	1	$\in (0, 1)$
PL-BP in (18)	1	$\in (0, 1)$	$\in (0, 1)$
LP in (22)	$\in (0, 1)$	0	$\in (0, 1)$
HP in (26)	$\in (0, 1)$	α	$\in (0, 1)$
BP from (30)	$\in (0, 1)$	$\in (0, 1)$ and $\beta < \alpha$	$\in (0, 1)$

IV. SINGLE CFOA IMPLEMENTATION OF NON-INTEGER ORDER FILTERS

A. IMPLEMENTATION OF FRACTIONAL-ORDER FILTERS

Using a CFOA as the active element, the corresponding filter topologies that implement the transfer functions in (1),

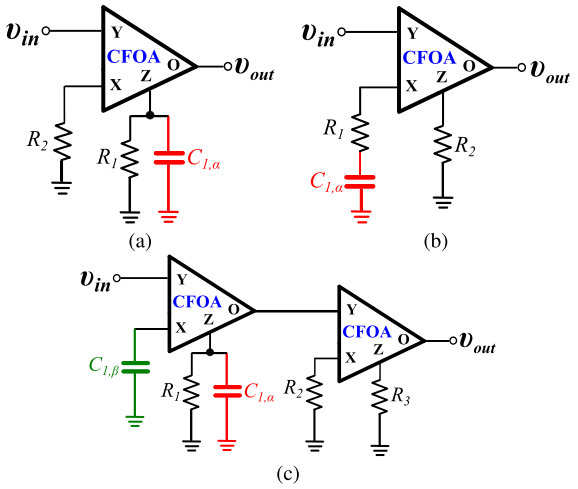

FIGURE 1. CFOA based realization of fractional-order (a) low-pass, (b) high-pass and (c) band-pass filters described by (1), (4) and (7).

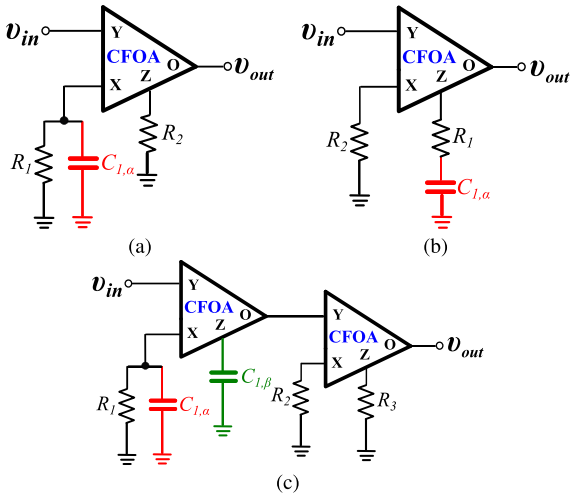

FIGURE 2. CFOA based realization of inverse fractional-order (a) low-pass, (b) high-pass, and (c) band-pass filters described by (9), (10), and (11).

(4), and (7) are depicted in Fig.1. As the impedance of a fractional-order capacitor (FOC) of order $0 < \alpha < 1$ is given by $Z = 1/C_\alpha s^\alpha$, the resulting transfer functions implemented by the topologies in Fig.1 are

$$H_{LP,FO}(s) = \frac{R_1}{R_2} \cdot \frac{1}{\left[(R_1 C_{1,\alpha})^{1/\alpha} s\right]^\alpha + 1}, \tag{32}$$

$$H_{HP,FO}(s) = \frac{R_2}{R_1} \cdot \frac{\left[(R_1 C_{1,\alpha})^{1/\alpha} s\right]^\alpha}{\left[(R_1 C_{1,\alpha})^{1/\alpha} s\right]^\alpha + 1}, \tag{33}$$

$$H_{BP,FO}(s) = \frac{R_3}{R_2} \cdot \frac{\left[(R_1 C_{1,\beta})^{1/\beta} s\right]^\beta}{\left[(R_1 C_{1,\alpha})^{1/\alpha} s\right]^\alpha + 1}. \tag{34}$$

Comparing (1), (4), and (7) with (32), (33), and (34) respectively, the associated design equations are summarized as

$$G_0 = \frac{R_1}{R_2} \qquad \tau = (R_1 C_{1,\alpha})^{1/\alpha}, \tag{35}$$

$$G_0 = \frac{R_2}{R_1} \qquad \tau = (R_1 C_{1,\alpha})^{1/\alpha}, \tag{36}$$

$$G_0 = \frac{R_3}{R_2} \qquad \tau = (R_1 C_{1,\alpha})^{1/\alpha} = (R_1 C_{1,\beta})^{1/\beta}. \tag{37}$$

These topologies offer the capability of cascade connection because of the high-impedance input and low-impedance output terminals, making use of the built-in CFOA buffer.

For the purpose of completeness, the corresponding implementations of the inverse filter functions are demonstrated in Fig.2, where it is readily verified that they are derived just by interchanging the impedances associated with terminals X and Z of the CFOA. The realized transfer functions have the form of (9), (10) and (11) leading to the design equations (35)–(36) slightly modified as follows: $G_0 = R_2/R_1$, and $G_0 = R_1/R_2$ while (35)–(37) remain unchanged.

B. IMPLEMENTATIONS OF POWER-LAW FILTERS

As the transfer functions in (12) and (15) are not realizable by fractional-order capacitors because of the absence of pure

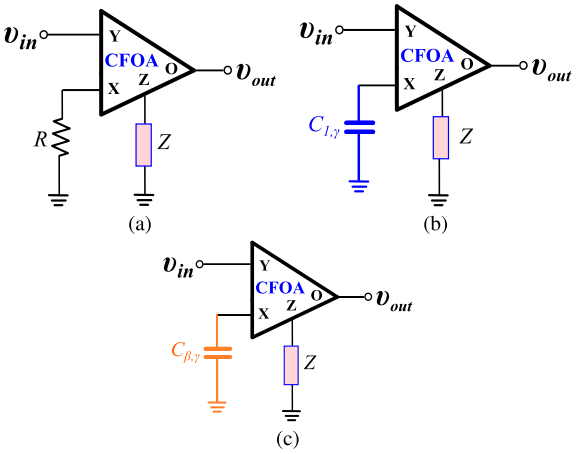

FIGURE 3. CFOA based realization of power-law (a) low-pass, (b) high-pass and (c) band-pass filters described by (12), (15) and (18).

Laplacian operators raised to a non-integer order, a method for realizing these functions is by employing appropriate power-law impedances [17]. The resulting realizations of the low-pass, high-pass, and band-pass filters are shown in Fig.3, with $Z = R/(\tau s + 1)^\gamma$ (R is an arbitrary value resistance) and the impedances of the fractional-order capacitors are given by: $Z_{1,\gamma} = R/G_0(\tau s)^\gamma$ and $Z_{1,\beta\gamma} = R/G_0(\tau s)^{\beta\gamma}$, respectively. It must be mentioned that these topologies preserve the cascadability feature observed in the case of the presented fractional-order filter structures.

The impedances of the fractional-order capacitors are approximated using the well-known approximation tools, such as the continued fraction expansion method. Assuming an n^{th}-order of approximation, the resulting rational integer-order impedance approximation function has the form in (38)

$$Z_{approx}(s) \simeq \frac{B_n s^n + B_{n-1} s^{n-1} + \ldots + B_1 s + B_0}{s^n + A_{n-1} s^{n-1} + \ldots + A_1 s + A_0}, \tag{38}$$

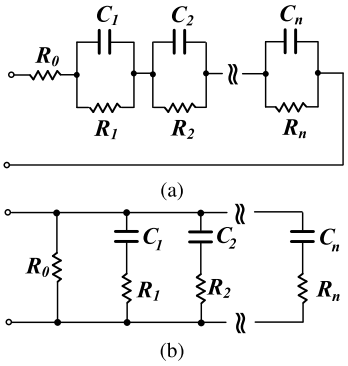

FIGURE 4. Foster RC networks for approximating non-integer impedances (a) type-I network, and (b) type-II network.

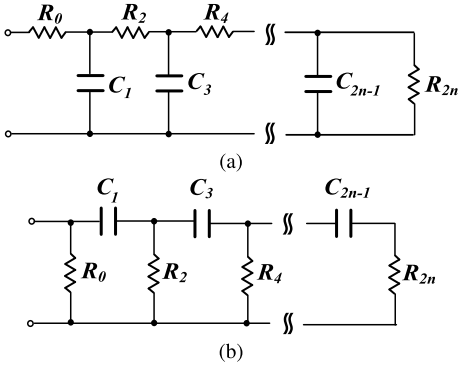

FIGURE 5. Cauer RC networks for approximating non-integer impedances (a) type-I network, and (b) type-II network.

with A_i and B_j ($i = 0, 1 \ldots n-1$ $j = 0, 1..n$) being positive and real coefficients.

The impedance function in (38) can be implemented by the Foster or Cauer networks depicted in Figs.4–5. The design equations of the Foster type-I and type-II networks in Fig.4 are given by

$$R_0 = B_n \; R_i = \frac{r_i}{|p_i|} \qquad C_i = \frac{1}{r_i}, \quad (i = 1, 2 \ldots n), \tag{39}$$

$$R_0 = \frac{1}{B_n} \; R_i = \frac{1}{r_i} \qquad C_i = \frac{r_i}{|p_i|}, \quad (i = 1, 2 \ldots n), \tag{40}$$

with r_i and p_i being the residues and poles of $Z_{approx}\,(s)$.

The corresponding design equations of the Cauer type-I and type-II networks in Fig.5 are summarized in (41) and (42) respectively.

$$R_0 = q_0 R_i = q_i C_j = q_j, \;\; i = 2, 4 \ldots 2n \; j = 1, 3 \ldots 2n-1, \tag{41}$$

$$R_0 = \frac{1}{q_0} R_i = \frac{1}{q_i} C_j = \frac{1}{q_j}, \;\; i = 2, 4 \ldots 2n \; j = 1, 3 \ldots 2n-1, \tag{42}$$

where $q_{i(j)}$ are the coefficients of the continued fraction expansion of the $Z_{approx}\,(s)$ in (38) [19].

The impedance of the general form $R/(\tau s+1)^{\gamma}$ has a low-pass filter behavior and can be also implemented by Cauer/Foster RC networks. In order to make this clear, let us consider for example the expression of the impedance of a Foster type-I network

$$Z(s) = R_0 + \sum_{i=1}^{n} R_i \frac{1}{\tau_i s + 1}. \tag{43}$$

The impedance function in (43) has a maximum value at low-frequencies equal to $R_0 + R_1 + \ldots + R_n$, while at high-frequencies it converges to R_0. In the intermediate range it monotonically decreases, providing a low-pass type frequency response. Therefore, choosing appropriate values of the *knee* frequencies, as well as of the frequency range of interest, this network is efficient towards this purpose. This will be performed by fitting the magnitude and phase response of the impedance [17], and the resulting approximation function will have the form of (38).

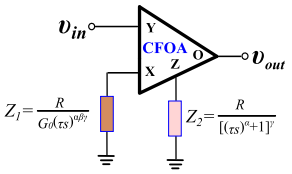

FIGURE 6. CFOA based generalized topology for implementing non-integer (fractional-order and power-law) order filter functions.

TABLE 2. Values of impedances in Fig.6 for implementing different types of the non-integer order filter functions ($\beta \leq \alpha$ and $0 \leq \alpha, \beta, \gamma \leq 1$).

Transfer Function	Impedance Z_1	Impedance Z_2
FO-LP in (1)	$\frac{R}{G_0}$	$\frac{R}{(\tau s)^{\alpha}+1}$
FO-HP in (4)	$\frac{R}{G_0(\tau s)^{\alpha}}$	$\frac{R}{(\tau s)^{\alpha}+1}$
FO-BP in (7)	$\frac{R}{G_0(\tau s)^{\beta}}$	$\frac{R}{(\tau s)^{\alpha}+1}$
PL-LP in (12)	$\frac{R}{G_0}$	$\frac{R}{(\tau s+1)^{\gamma}}$
PL-HP in (15)	$\frac{R}{G_0(\tau s)^{\gamma}}$	$\frac{R}{(\tau s+1)^{\gamma}}$
PL-BP in (18)	$\frac{R}{G_0(\tau s)^{\beta\gamma}}$	$\frac{R}{(\tau s+1)^{\gamma}}$
LP in (22)	$\frac{R}{G_0}$	$\frac{R}{[(\tau s)^{\alpha}+1])^{\gamma}}$
HP in (26)	$\frac{R}{G_0(\tau s)^{\alpha\gamma}}$	$\frac{R}{[(\tau s)^{\alpha}+1]^{\gamma}}$
BP from (30)	$\frac{R}{G_0(\tau s)^{\beta\gamma}}$	$\frac{R}{[(\tau s)^{\alpha}+1]^{\gamma}}$

C. IMPLEMENTATION OF GENERALIZED NON-INTEGER ORDER FILTERS

The generalized structure, capable of implementing all the aforementioned filters functions, is depicted in Fig.6, where $Z_1 = R/G_0(\tau s)^{\alpha\beta\gamma}$ and $Z_2 = R/[(\tau s)^{\alpha}+1]^{\gamma}$. Employing the results of Table 1, the expressions of the impedances Z_1 and Z_2 are summarized in Table 2. In order to implement the corresponding inverse filter functions, the impedances Z_1 and Z_2 must be interchanged in Fig.6, keeping their initial values. Inspecting the expressions in Table 2, it is readily obtained that the kind of the transfer function is excursively determined by the expression of the impedance Z_2, while the type of the filter function is determined through Z_1. More specifically:

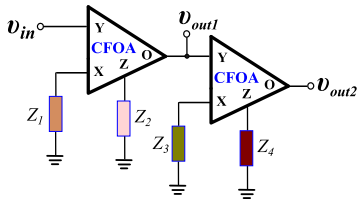

FIGURE 7. Generalized single-input multiple-output non-integer order filter topology.

TABLE 3. Values of passive elements of the foster type-i network in Fig.4a for implementing fractional-order low-pass (α=0.8, β=0, γ=1, and G_0=1), high-pass (α=0.8, β=0.8, γ=1, and G_0=1), and band-pass (α=0.8, β=0.5, γ=1, and G_0 = 1.584) filter functions.

Element	Z_2	Z_1(high-pass)	Z_1(band-pass)
R_0 (kΩ)	0.0715	0.113	0.442
R_1 (kΩ)	0.487	0.866	1.24
R_2 (kΩ)	2.1	3.24	2.61
R_3 (kΩ)	4.75	13.3	6.19
R_4 (kΩ)	2.1	64.9	17.8
R_5 (kΩ)	0.487	2870	118
C_1 (nF)	11.5	14.7	4.75
C_2 (nF)	15.4	29.4	19.1
C_3 (nF)	21	42.2	47.5
C_4 (nF)	150	56.2	110
C_5 (nF)	3740	27.4	196

- For $Z_2 = R/[(\tau s)^\alpha + 1]$, fractional-order filter functions are implemented, while the type of the function (i.e., low-pass, high-pass, and band-pass) is determined by the form of the impedance Z_1.
- For $Z_2 = R/[\tau s + 1]^\gamma$, power-law filter functions are implemented, while the type of the function (low-pass or high-pass) is determined by the form of the impedance Z_1.
- For $Z_2 = R/[(\tau s)^\alpha + 1]^\gamma$ generalized filter functions are implemented, and the determination of their type is performed through Z_1.

From the above, it is obvious that the generalized structure in Fig.6 offers design versatility and flexibility.

The topology in Fig.6 can be further enhanced for implementing a fractional-order single-input multiple-output (SIMO) filter structure, as demonstrated in Fig.7, where the realized transfer function is

$$H_{SIMO}(s) = \frac{Z_2 Z_4}{Z_1 Z_3}. \tag{44}$$

The expressions of impedances Z_1, Z_2 and Z_3, Z_4 can be chosen using the Table 2 for implementing the desired filter functions at the outputs of the structure.

V. SIMULATION AND EXPERIMENTAL RESULTS

The behavior of the filters is evaluated using the OrCAD PSpice suite, and the CFOA is simulated using the model of the AD844 discrete component [26]. The AD844 is biased at ±10V and the power dissipation of the structure is 130.1mW.

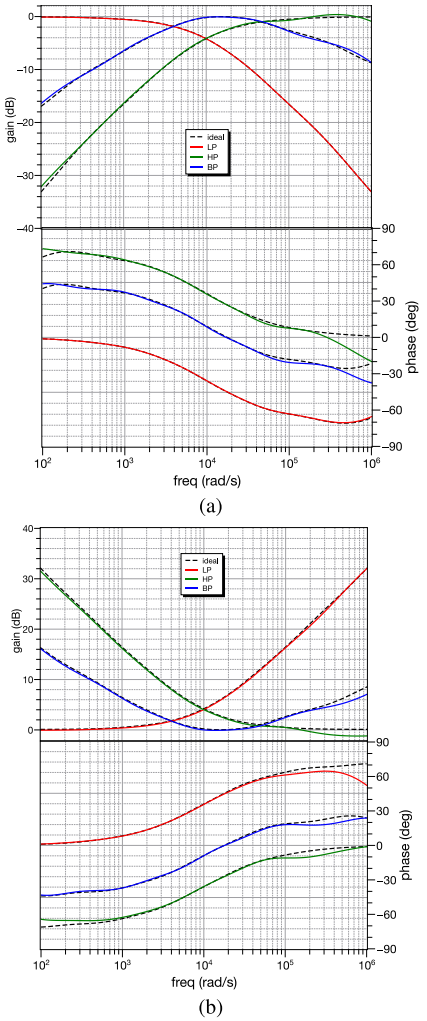

FIGURE 8. Gain and phase frequency responses of the designed (a) fractional-order low-pass (α=0.8, β=0, γ=1, and G_0=1), high-pass (α=0.8, β=0.8, γ=1, and G_0=1), band-pass (α=0.8, β=0.5, γ=1, and G_0=1.584) filters, and (b) their inverse counterparts.

A. SIMULATION RESULTS

1) FRACTIONAL-ORDER FILTERS

Considering that ω_p=1/τ=10krad/s, G_0=1, α=0.8, β={0,0.8,0.5}, γ=1, and R=10k Ω, the values of passive elements of the Foster type-I network in Fig.4a, for approximating Z_1 and Z_2 in the range [10^2,10^6]rad/s, are summarized in Table 3. These values are rounded to the E96 series defined in IEC 60063.

The derived gain and phase responses are demonstrated in the plots of Fig.8a, accompanied by the theoretical plots given by dashes. The values of the *knee* frequency and of the phase at this frequency are {6.97krad/s, −29.7°} for the low-pass filter and {14.74krad/s, 27.5°} for the high-pass filter. The corresponding theoretical predicted values are {6.84krad/s, −29.7°} and {14.63krad/s, 29.73°}, respectively. With regards to the band-pass filter, the values of the peak frequency, gain at peak frequency, and bandwidth are simulated as {14.75krad/s, −0.06dB, 119.76krad/s},

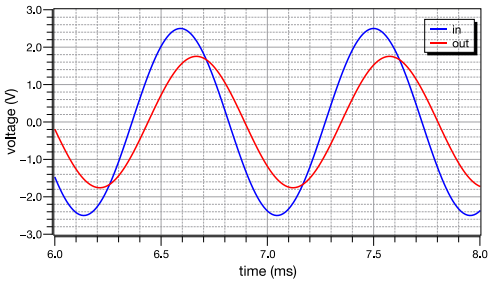

FIGURE 9. Time-domain behavior of the fractional-order low-pass filter for $5V_{p\text{-}p}$ input stimulation at the *knee* frequency.

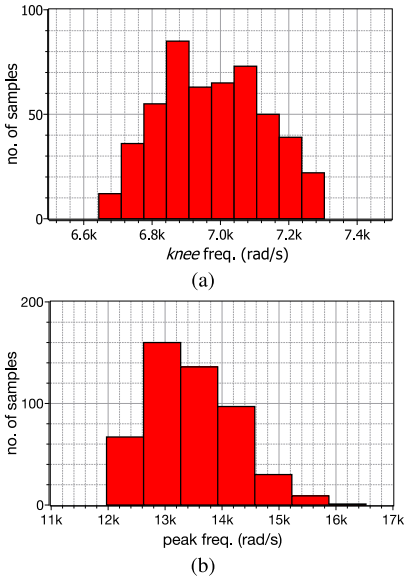

FIGURE 10. Monte-Carlo analysis results of (a) the *knee* frequency of the low-pass fractional-order filter, and (b) the peak frequency of the fractional-order band-pass filter.

close to the theoretically predicted ones {15.5krad/s, 0dB, 124.5krad/s}.

The inverse filter transfer functions are realized by interchanging the impedances associated with the X and Z terminals of the CFOA. Following this, the derived frequency responses are depicted in Fig.8b, where the *knee* frequency (i.e., the frequency where a +3dB rise of the gain from its minimum value is observed) and the phase at this frequency are {7.11krad/s, 30.1°} and {14.5krad/s, −30.6°}, for the inverse low and high-pass filters, while the corresponding values expected from the theory are {6.84krad/s, 29.7°} and {14.62krad/s, -29.73°}, respectively. The simulated values of the peak frequency, gain at peak frequency, and bandwidth of the inverse band-pass filter are {14.74krad/s, −0.1dB, 118.45krad/s}, with the associated theoretical values being {15.5krad/s, 0dB, 124.5krad/s}.

The time-domain behavior of the filters is evaluated in the case of the low-pass filter, by stimulating it with a sinusoidal $5V_{p\text{-}p}$ signal at its *knee* frequency. The observed input and output waveforms are demonstrated in Fig.9, where the gain

TABLE 4. Values of passive elements of the foster type-i network in Fig.4a for implementing power-law low-pass (α=1, β=0, γ=0.8, and G_0=1), high-pass (α=1, β=1, γ=0.8, and G_0=1), and band-pass (α=1, β=0.5, γ=0.8, and G_0=1.326) filter functions.

Element	Z_2	Z_1(high-pass)	Z_1(band-pass)
R_0 (kΩ)	0.0316	0.113	0.887
R_1 (kΩ)	0.14	0.866	1.74
R_2 (kΩ)	0.348	3.24	3.01
R_3 (kΩ)	0.787	13.3	5.76
R_4 (kΩ)	1.82	64.9	13.7
R_5 (kΩ)	6.81	2870	61.9
C_1 (nF)	12.4	14.7	2.67
C_2 (nF)	23.2	29.4	13.7
C_3 (nF)	31.6	42.2	41.2
C_4 (nF)	32.4	56.2	113
C_5 (nF)	14	27.4	274

is −3dB and the phase difference between the output and input waveforms is −29.7°. Applying a sinusoidal stimulus with frequency equal to $0.1\omega_{-3dB}$ and variable amplitude, the *rms* value of the input signal for observing 1% Total Harmonic Distortion (THD) at the output is equal to 4.83V. Integrating the noise over the pass-band of the filter, the *rms* value of the input referred noise is 8.3 μV. According to these results, the predicted value of the *dynamic range* of the filter will be 115.3dB.

Employing the Monte-Carlo analysis, which is available by the *Advanced Analysis* tool of the OrCAD PSpice and considering a random deviation of the passive elements values from their nominal ones within the range ±5%, the statistical plots (N=500 runs) associated with the *knee* frequency of the low-pass filter and the peak frequency of the band-pass filter are provided in Fig.10. The values of the standard deviation are 0.15krad/s and 0.77krad/s, respectively.

2) POWER-LAW FILTERS

The values of passive elements of the Foster type-I network in Fig.4 for implementing the frequency dependent impedance Z_2 in the case of power-law filters with α=1, β={1,0.5}, γ=0.8, and $\omega_p = 1/\tau$=10krad/s, are summarized in Table 4. It must be mentioned at this point that the values of elements for implementing Z_1 in the case of high-pass filter are the same as in the case of the corresponding fractional-order filter.

The simulated gain the phase responses are demonstrated in the plots of Fig.11a, accompanied by the theoretical plots given by dashes. The values of the *knee* frequency and of the phase at this frequency are {11.98krad/s, -39.6°} for the low-pass filter and {8.64krad/s, 39.9°} for the high-pass filter. The corresponding theoretical predicted values are {11.74krad/s, -39.66°} and {8.52krad/s, 39.65°}, respectively. With regards to the band-pass filter, the values of the peak frequency, gain at peak frequency, and bandwidth are simulated as {9.95krad/s, -0.06dB, 45.7krad/s}, close to the theoretically predicted ones {10krad/s, 0dB, 43.1krad/s}.

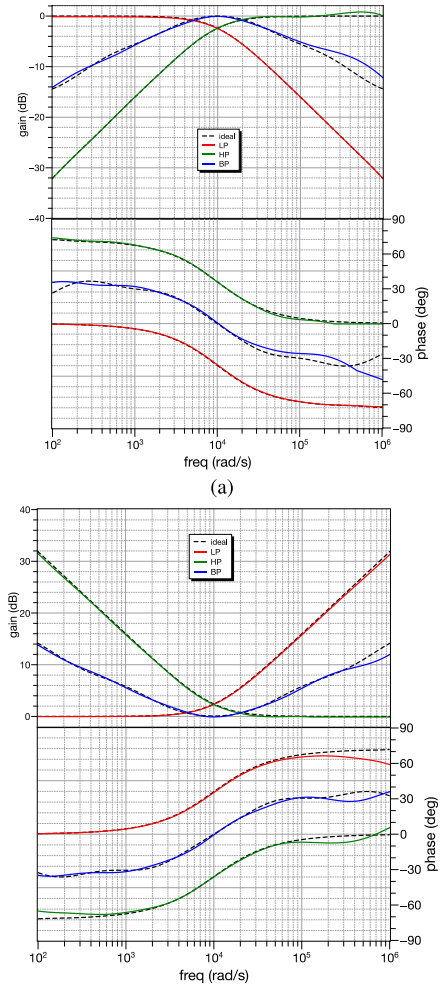

FIGURE 11. Gain and phase frequency responses of the designed power-law (a) low-pass (α=1, β=0, γ=0.8, and G_0=1), high-pass (α=1, β=1, γ=0.8, and G_0=1), and band-pass (α=1, β=0.5, γ=0.8, and G_0=1.326) filters and (b) their inverse counterparts.

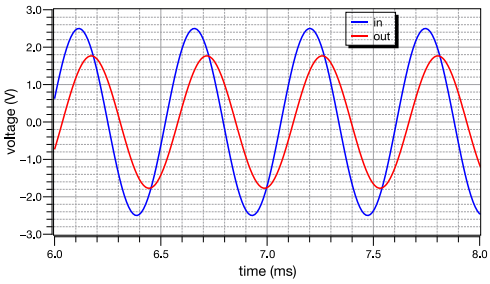

FIGURE 12. Time-domain behavior of the power-law low-pass filter for $5V_{p\text{-}p}$ input stimulation at the *knee* frequency.

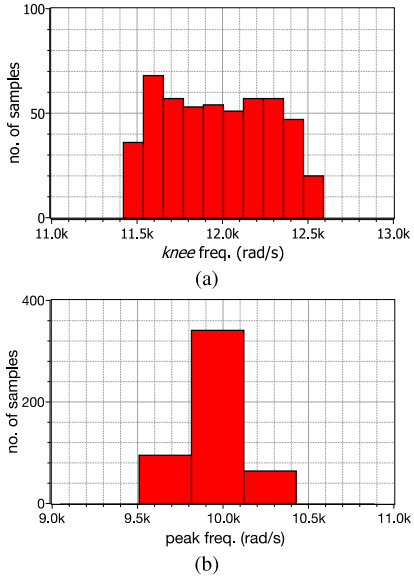

FIGURE 13. Monte-Carlo analysis results of (a) the *knee* frequency of the power-law low-pass filter, and (b) the peak frequency of the power-law band-pass filter.

The frequency responses of the inverse filter functions are depicted in Fig.11b, where the *knee* frequency and the phase at this frequency are {11.97krad/s, 39.4°} and {8.29krad/s, -40°}, for the inverse low and high-pass filters, with the theoretically predicted values being {11.74krad/s, 39.6°} and {8.52krad/s, -39.65°}, respectively. The values of the peak frequency, gain at peak frequency, and bandwidth of the band-pass filter are {9.95krad/s, -0.1dB, 42.1krad/s}, close to the theoretically predicted ones {10krad/s, 0dB, 43.1krad/s}.

The time-domain behavior of the low-pass filter is demonstrated in Fig.12, where the gain is -3dB and the phase difference between the output and input waveforms is equal to -39.2°. The *rms* value of the input signal ($0.1\omega_{-3dB,LP}$) for 1% THD level is equal to 4.7V. The *rms* value of the input referred integrated noise is 6.96 μV and, therefore, the *dynamic range* of the filter will be 116.6dB.

The statistical histograms of the *knee* frequency of the low-pass filter and the peak frequency of the band-pass filter are provided in Fig.13, where the values of the standard deviation are 0.31krad/s and 0.26krad/s, respectively.

3) GENERALIZED FILTERS

The values of passive elements of the Foster type-I network in Fig.4a for implementing the frequency dependent impedance Z_2 in the case of a generalized non-integer order filter with α=0.8, β={0,0.8,0.5}, γ=0.8, and $\omega_p = 1/\tau$=10krad/s, are summarized in Table 5.

The derived gain and phase responses of the low-pass and high-pass filters are demonstrated in the plots of Fig.14a, with the *knee* frequency and phase at this frequency being {7.91krad/s, -29.3°} for the low-pass filter and {12.85krad/s, 29.9°} for the high-pass filter. The corresponding theoretically predicted values are {8.82krad/s, -27.14°} and {11.3krad/s, 27.17°}, respectively. With regards to the behavior of the band-pass filter, the values of the peak frequency, gain at peak frequency, and bandwidth are simulated as {14.1krad/s, -0.11dB, 173.4krad/s}, with the theoretical valued being {14.9krad/s, 0dB, 181.6krad/s}.

TABLE 5. Values of passive elements of the foster type-i network in Fig.4a for implementing generalized low-pass (α=0.8, β=0, γ=0.8, and G_0=1), high-pass (α=0.8, β=0.8, γ=0.8, and G_0=1), and band-pass (α=0.8, β=0.5, γ=0.8, and G_0=1.445) filter functions.

Element	Z_2	Z_1(high-pass)	Z_1(band-pass)
R_0 (kΩ)	0.215	0.324	0.825
R_1 (kΩ)	0.825	1.5	1.58
R_2 (kΩ)	2.21	4.12	2.74
R_3 (kΩ)	4.22	12.7	5.23
R_4 (kΩ)	2	46.4	12.7
R_5 (kΩ)	0.453	604	56.2
C_1 (nF)	4.42	5.76	2.87
C_2 (nF)	10.2	16.5	14.7
C_3 (nF)	19.1	31.6	45.3
C_4 (nF)	127	56.2	124
C_5 (nF)	3400	60.4	301

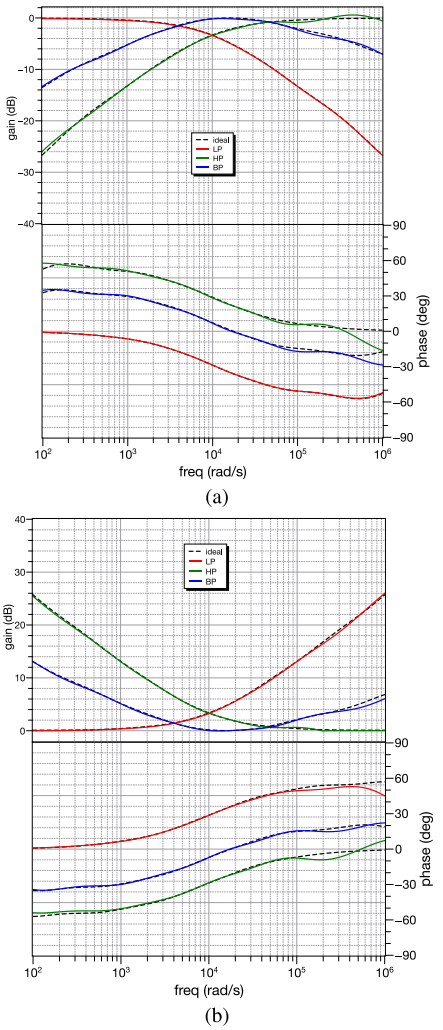

FIGURE 14. Gain and phase frequency responses of the designed generalized (a) low-pass (α=0.8, β=0, γ=0.8, and G_0=1), high-pass (α=0.8, β=0.8, γ=0.8, and G_0=1), band-pass (α=0.8, β=0.5, γ=0.8, and G_0=1.445) filters, and (b) of the corresponding inverse filters.

The frequency behavior of the inverse filters is depicted in Fig.14b, where the *knee* frequency and the phase at this frequency being {7.1krad/s, 29.2°} and {14.4krad/s, -29.8°}, for the inverse low and high-pass filters, while the corresponding values expected from the theory are {8.82krad/s, 27.14°} and {11.3krad/s, -27.17°}, respectively. The simulated values of the peak frequency, gain at peak frequency, and bandwidth of the inverse band-pass filter are {13.2krad/s, -0.05dB, 178.5krad/s}, with the associated theoretical values being {14.9krad/s, 0dB, 181.6krad/s}.

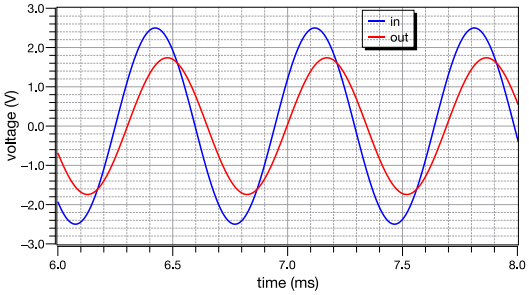

FIGURE 15. Time-domain behavior of the generalized low-pass filter for $5V_{p\text{-}p}$ input stimulation at the *knee* frequency.

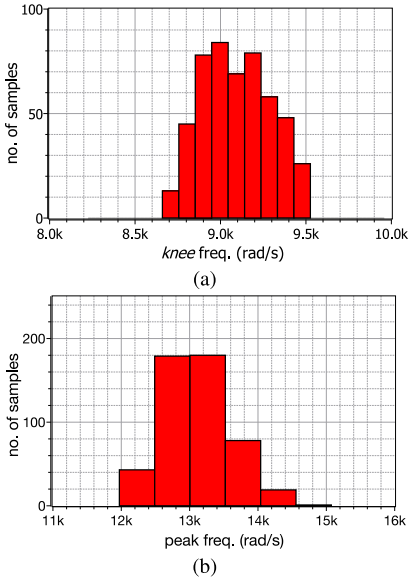

FIGURE 16. Monte-Carlo analysis results of (a) the *knee* frequency of the generalized low-pass filter, and (b) the peak frequency of the generalized band-pass filter.

In Fig.15 the input and output waveforms in the case of a low-pass filter are depicted, with the gain being equal to −3dB and the phase difference between the output and input waveforms being -29.7°. The linearity performance of the filter is evaluated under the same conditions as before, and the *rms* value of the input signal for level of THD equal to 1% is 4.86V. The input referred integrated noise has *rms* value equal to 10.2 μV, resulting a 113.5dB *dynamic range*.

The statistical results about the *knee* frequency of the low-pass filter and the peak frequency of the band-pass filter are demonstrated in Fig.16, with the values of the standard deviation being 0.2krad/s for the low-pass filter and

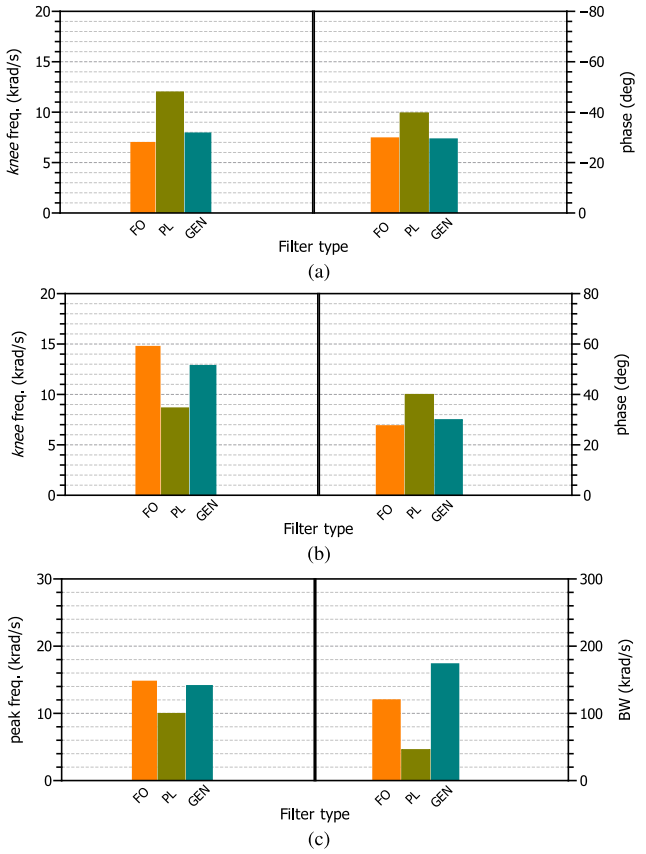

FIGURE 17. Performance comparison results about the most important frequency characteristics of the (a) low-pass, (b) high-pass, and (c) band-pass generalized filters.

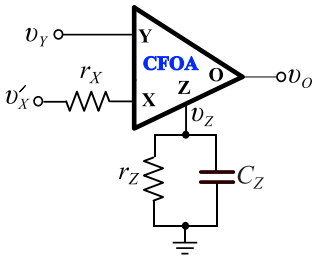

FIGURE 18. CFOA macro-model including the parasitic elements.

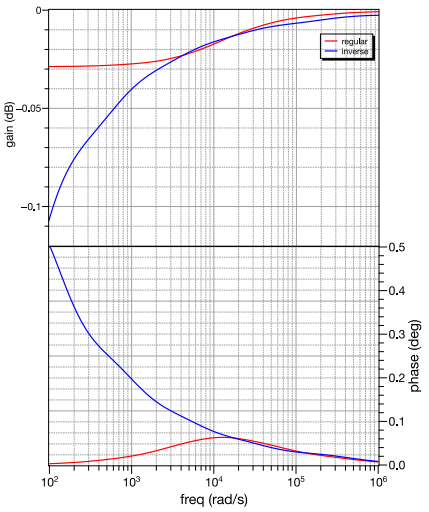

FIGURE 19. Gain and phase responses of the error factors in (46)–(47).

0.58krad/s for the band-pass filter, while the associated mean values are 9.09krad/s and 13.1krad/s, respectively.

The performance of the designed low-pass filters is evaluated by the charts in Fig.17a, where it is derived that the fractional-order filter offers the lowest *knee* frequency while the power-law offers the highest one among the filters under consideration. With regards to the phase at the *knee* frequency, the power-law filter offers the maximum change while the fractional-order and the generalized filters offers comparable changes. Considering the high-pass filters, then from the charts in Fig.17b it is obtained that the fractional-order filter offers the highest *knee* frequency while the power-law offers the lowest one, whereas for the phase the same derivation as before is obtained. According to the charts in Fig.17c, which correspond to the case of the band-pass filters, it is concluded that the power-law filter offers the lowest peak frequency, and the fractional-order and generalized filters offer comparable values of the peak frequency. The generalized filter offers the maximum bandwidth, while the lowest one bandwidth is offered by the power-law filter.

In order to evaluate the effect of the CFOA non-idealities on the performance of the filters, let us consider the the macro-model of the AD844 depicted in Fig.18. According to [26], the values of parasitic elements are: r_X=50 Ω, r_Z=3M Ω, and C_Z=4.5pF. Ignoring the effect of the parasitic capacitance, the transfer function realized by the topology in Fig.6 is

$$H_{real}(s) = \frac{Z_2 r_Z}{(Z_2 + r_Z)(Z_1 + r_X)}. \tag{45}$$

Using the values in Table 2 and assuming that $Z_1 \gg r_X$, the transfer function in (45) becomes

$$H_{real}(s) = H_{ideal}(s) \frac{\frac{r_Z}{R}\{[(\tau s)^\alpha + 1]\}^\gamma}{\frac{r_Z}{R}\{[(\tau s)^\alpha + 1]\}^\gamma + 1}, \tag{46}$$

with $H_{ideal}(s) = Z_2/Z_1$, being the transfer function which corresponds to the case of an ideal CFOA.
Following a similar procedure in the case of inverse filters, the resulting transfer function will be

$$H'_{real}(s) = H_{ideal}(s) \frac{\frac{G_0 r_Z}{R}(\tau s)^{\beta\gamma}}{\frac{G_0 r_Z}{R}(\tau s)^{\beta\gamma} + 1} \tag{47}$$

Employing in (46)–(47) the parameters values which are considered in the design examples, the frequency behavior of the extra scaling factors is demonstrated in Fig.19, where it is evident that it does not significantly affect the responses of the filters.

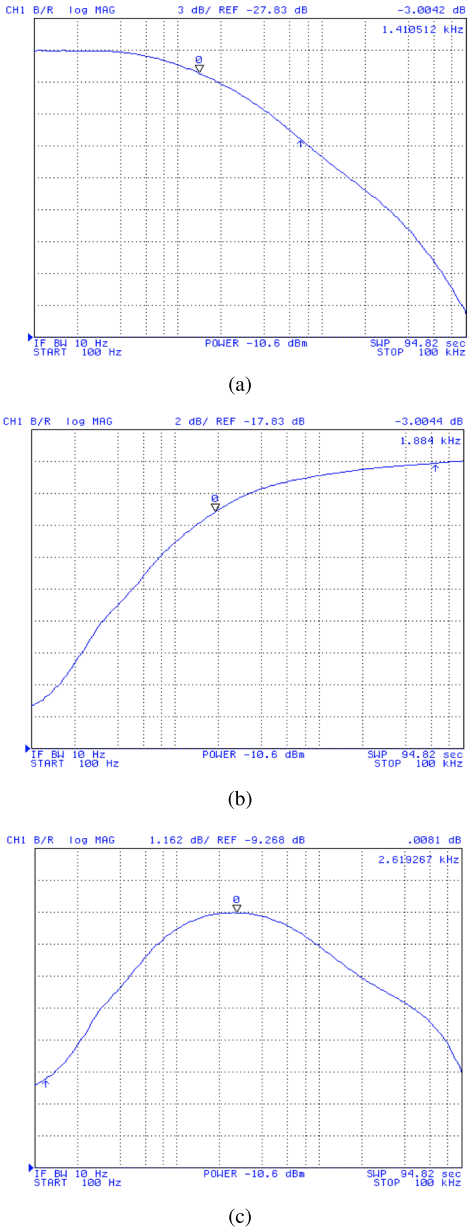

FIGURE 20. Experimental frequency responses of the designed generalized (a) low-pass (α=0.8, β=0, γ=0.8, and G_0=1), (b) high-pass (α=0.8, β=0.8, γ=0.8, and G_0=1), and (c) band-pass (α=0.8, β=0.5, γ=0.8, and G_0=1.445) filters.

B. EXPERIMENTAL RESULTS

The responses of the generalized low-pass, high-pass, and band-pass filters obtained through the utilization of the HP 4395A Network/Spectrum analyzer are depicted in Figs.20a–20c, respectively. The *knee* frequencies of the low-pass and high-pass filters are 8.86krad/s and 11.6krad/s close to the theoretical values 8.82krad/s and 11.3krad/s, respectively. The center frequency and the gain at this frequency of the band-pass filer are 16.46krad/s and 0.01dB, close to the theoretically predicted ones values 14.9krad/s and 0dB.

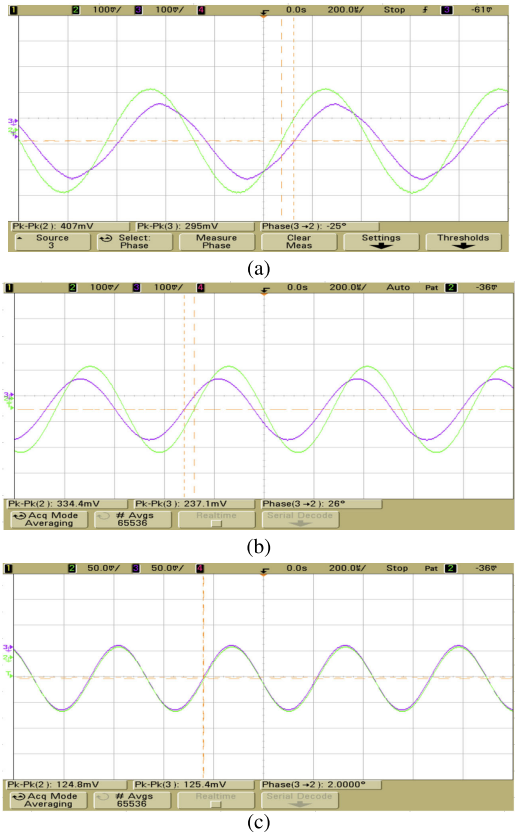

FIGURE 21. Input and output waveforms of the proposed generalized (a) low-pass, (b) high-pass filters, stimulated at their *knee* frequency, and (c) band-pass filter, stimulated at its center frequency.

Also, the measured bandwidth is 178.4krad/s with the value predicted from the theory being 181.6krad/s.

The filters have been also experimentally tested by stimulating the low-pass and high-pass filter topologies at their *knee* frequencies 7.91krad/s and 12.85krad/s, respectively. The waveforms obtained through an Agilent DSO6034A oscilloscope are demonstrated in Figs.21a–21b where the measured values of the gain and phase are {-2.79dB, -25^o} and {-2.99dB, 26^o}, close to the theoretically predicted ones {-3dB, -27.14^o} and {-3dB, 27.17^o}. In the case of the band-pass filter, the resulting input and output waveforms for a stimulation input at the center frequency 14.9krad/s are depicted in Fig.21c, where the gain and phase are {0dB, 2^o} with those expected by the theory being {0dB, 1.8^o}.

VI. CONCLUSION

A CFOA based implementation of a generalized filter structure which is capable of deriving both the fractional-order and power-law filter functions, as well of their inverse filter functions counterparts was proposed offering many attractive features including cascadability. The presented simulation and experimental results confirm the proper performance in terms of accuracy and sensitivity making them attractive candidates for non-integer order signal processing systems. As this study is focused on filter functions of orders less

than one, future research steps include the exploitation of the applicability of the presented concept in the case of high-order non-integer filters, as well as their possible implementation using programmable devices such as a suitable Field Programmable Analog Array (FPAA) device.

ACKNOWLEDGMENT

The publication of the article in OA mode was financially supported by HEAL-Link.

REFERENCES

[1] G. Tsirimokou, C. Psychalinos, and A. Elwakil, *Design of CMOS Analog Integrated Fractional-Order Circuits: Applications in Medicine and Biology*. Switzerland: Springer, 2017.

[2] A. Tepljakov, B. B. Alagoz, C. Yeroglu, E. A. Gonzalez, S. H. Hosseinnia, E. Petlenkov, A. Ates, and M. Cech, "Towards industrialization of FOPID controllers: A survey on milestones of fractional-order control and pathways for future developments," *IEEE Access*, vol. 9, pp. 21016–21042, 2021.

[3] J. Dvorak, L. Langhammer, J. Jerabek, J. Koton, R. Sotner, and J. Polak, "Synthesis and analysis of electronically adjustable fractional-order low-pass filter," *J. Circuits, Syst. Comput.*, vol. 27, no. 2, Feb. 2018, Art. no. 1850032.

[4] D. Kubanek, T. Freeborn, and J. Koton, "Fractional-order band-pass filter design using fractional-characteristic specimen functions," *Microelectron. J.*, vol. 86, pp. 77–86, Apr. 2019.

[5] S. Mahata, R. Kar, and D. Mandal, "Optimal fractional-order highpass Butterworth magnitude characteristics realization using current-mode filter," *AEU, Int. J. Electron. Commun.*, vol. 102, pp. 78–89, Apr. 2019.

[6] L. Langhammer, J. Dvorak, R. Sotner, J. Jerabek, and P. Bertsias, "Reconnection–less reconfigurable low–pass filtering topology suitable for higher–order fractional–order design," *J. Adv. Res.*, vol. 25, pp. 257–274, Sep. 2020.

[7] O. Domansky, R. Sotner, L. Langhammer, and L. Polak, "Electronically reconfigurable and tunable fractional-order filter using resonator concept and feedforward path for low-frequency tone signalization," *IEEE Access*, vol. 9, pp. 138026–138041, 2021.

[8] O. Sladok, J. Koton, D. Kubanek, J. Dvorak, and C. Psychalinos, "Pseudo-differential $(2 + \alpha)$-order Butterworth frequency filter," *IEEE Access*, vol. 9, pp. 92178–92188, 2021.

[9] G. Varshney, N. Pandey, and R. Pandey, "Generalization of shadow filters in fractional domain," *Int. J. Circuit Theory Appl.*, vol. 49, no. 10, pp. 3248–3265, Oct. 2021.

[10] S. Mahata, N. Herencsar, and D. Kubanek, "Further generalization and approximation of fractional-order filters and their inverse functions of the second-order limiting form," *Fractal Fractional*, vol. 6, no. 4, p. 209, Apr. 2022.

[11] A. Soni and M. Gupta, "Designing of fractional order Bessel filter using optimization techniques," *Int. J. Electron. Lett.*, vol. 10, no. 1, pp. 71–86, Jan. 2022.

[12] S. Kapoulea, C. Psychalinos, and A. S. Elwakil, "Power law filters: A new class of fractional-order filters without a fractional-order Laplacian operator," *AEU, Int. J. Electron. Commun.*, vol. 129, Feb. 2021, Art. no. 153537.

[13] R. Malatesta, S. Kapoulea, C. Psychalinos, and A. S. Elwakil, "Design of low-voltage FO-[PD] controller for motion systems," *J. Low Power Electron. Appl.*, vol. 11, no. 2, p. 26, May 2021.

[14] S. Mahata, N. Herencsar, and D. Kubanek, "On the design of power law filters and their inverse counterparts," *Fractal Fractional*, vol. 5, no. 4, p. 197, Nov. 2021.

[15] N. Mijat, D. Jurisic, and G. S. Moschytz, "Analog modeling of fractional-order elements: A classical circuit theory approach," *IEEE Access*, vol. 9, pp. 110309–110331, 2021.

[16] J. Nako, C. Psychalinos, A. S. Elwakil, and D. Jurisic, "Design of higher-order fractional filters with fully controllable frequency characteristics," *IEEE Access*, vol. 11, pp. 43205–43215, 2023.

[17] J. Nako, C. Psychalinos, and A. S. Elwakil, "One active element implementation of fractional-order Butterworth and Chebyshev filters," *AEU, Int. J. Electron. Commun.*, vol. 168, Aug. 2023, Art. no. 154724.

[18] J. Nako, C. Psychalinos, and A. S. Elwakil, "Minimum active component count design of a $PI^{\lambda}D^{\mu}$ controller and its application in a cardiac pacemaker system," *J. Low Power Electron. Appl.*, vol. 13, no. 1, p. 13, Feb. 2023.

[19] G. Tsirimokou, "A systematic procedure for deriving RC networks of fractional-order elements emulators using MATLAB," *AEU, Int. J. Electron. Commun.*, vol. 78, pp. 7–14, Aug. 2017.

[20] P. Bertsias, G. Tsirimokou, C. Psychalinos, and A. S. Elwakil, "Fully electronically tunable inverse fractional-order filter designs," in *Proc. Novel Intell. Lead. Emerg. Sci. Conf. (NILES)*, vol. 1, Oct. 2019, pp. 42–45.

[21] P. Bertsias, C. Psychalinos, S. Minaei, A. Yesil, and A. S. Elwakil, "Fractional-order inverse filters revisited: Equivalence with fractional-order controllers," *Microelectron. J.*, vol. 131, Jan. 2023, Art. no. 105646.

[22] D. R. Bhaskar, M. Kumar, and P. Kumar, "Fractional order inverse filters using operational amplifier," *Anal. Integr. Circuits Signal Process.*, vol. 97, no. 1, pp. 149–158, Oct. 2018.

[23] D. R. Bhaskar, M. Kumar, and P. Kumar, "Minimal realization of fractional-order inverse filters," *IETE J. Res.*, vol. 68, no. 6, pp. 4626–4639, 2022.

[24] E. M. Hamed, L. A. Said, A. H. Madian, and A. G. Radwan, "On the approximations of CFOA-based fractional-order inverse filters," *Circuits, Syst., Signal Process.*, vol. 39, no. 1, pp. 2–29, Jan. 2020.

[25] A. Pagidas, C. Psychalinos, and A. S. Elwakil, "Field programmable analog array based non-integer filter designs," *Electronics*, vol. 12, no. 16, p. 3427, Aug. 2023.

[26] Analog Devices. *AD844 60 MHz 2000 V/us Monolithic Op Amp With Quad Low Noise, Data Sheet, Rev. G*. Accessed: Sep. 5, 2023. [Online]. Available: https://www.analog.com/en/products/ad844.html

JULIA NAKO (Graduate Student Member, IEEE) received the B.Sc. and M.Sc. degrees from the University of Patras, Greece, in 2021 and 2023, respectively, where she is currently pursuing the Ph.D. degree with the Postgraduate Studies Program "Electronics-Circuits and Systems," Physics Department. Her main research interests include the design of analog integrated circuits and systems for signal processing, including non-integer order circuits, control systems, and biomedical circuits. She is a member of the Electronics Laboratory, Analog VLSI Design Team, working under the supervision of Prof. Costas Psychalinos.

COSTAS PSYCHALINOS (Senior Member, IEEE) received the B.Sc. and Ph.D. degrees in physics and electronics from the University of Patras, Greece, in 1986 and 1991, respectively. From 1993 to 1995, he was a Postdoctoral Researcher with the VLSI Design Laboratory, University of Patras, where he was an Adjunct Lecturer with the Department of Computer Engineering and Informatics, from 1996 to 2000. From 2000 to 2004, he was an Assistant Professor with the Electronics Laboratory, Department of Physics, Aristotle University of Thessaloniki, Greece. Since 2004, he has been a Faculty Member of the Electronics Laboratory, Department of Physics, University of Patras. Currently, he is a full professor. His research areas are the development of CMOS analog integrated circuits, including fractional-order circuits and systems, continuous and discrete-time analog filters, amplifiers, and low voltage/low power building blocks for analog signal processing. He serves as the Editor-in-Chief for the Circuit and Signal Processing Section for the *Electronics* journal (MDPI). He serves as an Area Editor for the *International Journal of Electronics and Communications* (AEUE) and the *International Journal of Circuit Theory and Applications*. He is an Associate Editor of the *Circuits, Systems, and Signal Processing* and the *Journal of Advanced Research*. He is a member of the Editorial Board of the *Microelectronics Journal*, *Analog Integrated Circuits and Signal Processing Journal*, *IETE Journal of Education*, *Fractal and Fractional*, and *Journal of Low Power Electronics and Applications*. He is a member of the Nonlinear Circuits and Systems Technical Committee of the IEEE CAS Society.

AHMED S. ELWAKIL (Senior Member, IEEE) was born in Cairo, Egypt. He received the B.Sc. and M.Sc. degrees in electronics and communications from Cairo University, Egypt, and the Ph.D. degree in electrical and electronic engineering from the National University of Ireland, University College Dublin. He also held visiting positions with Istanbul Technical University, Turkey; Queens University, Belfast, U.K.; the Technical University of Denmark, Lyngby, Denmark; and the King Abdullah University of Science and Technology, Saudi Arabia. He is currently a Full Professor with the University of Sharjah, United Arab Emirates; also with the University of Calgary, AB, Canada; and also with the Nanoelectronics Integrated Systems Center (NISC) Research Center, Nile University, Cairo. He has authored or coauthored more than 350 publications in these areas (current H-index 45). His research interests include circuit theory, nonlinear dynamics, chaos theory, fractional-order circuits and systems with diverse applications ranging from the modeling of oscillatory networks and nonlinear behavior in electronic circuits and plasma physics to modeling of energy storage devices, bio-materials, and biological tissues. He has been a member of the IEEE Technical Committee on Nonlinear Circuits and Systems, since 2000. He was a recipient of the Egyptian Government First Class Medal for Achievements in Engineering Sciences, in 2015, and the UAE President Award (Khalifa Award), in 2020. He is also an International Observer in the European Cooperation in Science and Technology (COST) action on fractional-order system analysis synthesis and their importance for future design (CA15225) and an Expert with the United Nations Development Program (UNDP). He was on the editorial board of the IEEE JOURNAL ON EMERGING AND SELECTED TOPICS IN CIRCUITS AND SYSTEMS and an Associate Editor of IEEE TRANSACTIONS ON CIRCUITS AND SYSTEMS—I: REGULAR PAPERS. He currently serves as the Editor-in-Chief for the *International Journal of Circuit Theory and Applications* (Wiley) and an Associate Editor for the *International Journal of Electronics and Communications* (AEUE) (Elsevier).

SHAHRAM MINAEI (Senior Member, IEEE) received the B.Sc. degree in electrical and electronics engineering from the Iran University of Science and Technology, Tehran, Iran, in 1993, and the M.Sc. and Ph.D. degrees in electronics and communication engineering from Istanbul Technical University, Istanbul, Turkey, in 1997 and 2001, respectively. He is currently a Professor with the Department of Electrical and Electronics Engineering, Dogus University, Istanbul, Turkey. He has more than 190 publications in scientific journals or conference proceedings. His current research interests include current-mode circuits and analog signal processing. His published works have received more than 6000 citations and his current H-index is 42 in Google Scholar. He is an Editor of the *Journal of Circuits, Systems, and Computers* (JCSC), *International Journal of Circuit Theory and Applications* (IJCTA), and *Elektronika ir Elektrotechnika*. He is also the Editor-in-Chief of the *International Journal of Electronics and Communications* (AEU).